A SECOND ORDER ACCURATE EMBEDDED BOUNDARY METHOD FOR THE WAVE EQUATION WITH DIRICHLET DATA*

HEINZ-OTTO KREISS† AND N. ANDERS PETERSSON‡

Abstract. The accuracy of Cartesian embedded boundary methods for the second order wave equation in general two-dimensional domains subject to Dirichlet boundary conditions is analyzed. Based on the analysis, we develop a numerical method where both the solution and its gradient are second order accurate. We avoid the small-cell stiffness problem without sacrificing the second order accuracy by adding a small artificial term to the Dirichlet boundary condition. Long-time stability of the method is obtained by adding a small fourth order dissipative term. Several numerical examples are provided to demonstrate the accuracy and stability of the method. The method is also used to solve the two-dimensional TM_z problem for Maxwell's equations posed as a second order wave equation for the electric field coupled to ordinary differential equations for the magnetic field.

Key words. wave equation, stability, accuracy, embedded boundary

AMS subject classifications. 65M06, 65M12

DOI. 10.1137/040604728

1. Introduction. Consider the Dirichlet problem for the second order wave equation in a two-dimensional domain Ω with boundary Γ:

$$u_{tt} = \Delta u + F(\boldsymbol{x}, t), \quad \boldsymbol{x} \in \Omega, \quad t \geq 0, \tag{1}$$

$$u(\boldsymbol{x}, t) = f(\boldsymbol{x}, t), \quad \boldsymbol{x} \in \Gamma, \quad t \geq 0, \tag{2}$$

$$u(\boldsymbol{x}, 0) = u_0(\boldsymbol{x}), \quad \boldsymbol{x} \in \Omega, \tag{3}$$

$$u_t(\boldsymbol{x}, 0) = u_1(\boldsymbol{x}), \quad \boldsymbol{x} \in \Omega. \tag{4}$$

In this paper we continue the approach started in [1] and [2] and develop a numerical method that directly discretizes the second order wave equation. This approach is motivated by wave propagation problems from applications such as seismology, acoustics, and general relativity, where the underlying differential equations are systems of second order hyperbolic partial differential equations. For every second order hyperbolic system, there is an equivalent but larger first order hyperbolic system. For example, two-dimensional acoustic wave propagation is governed by a scalar second order wave equation for the pressure or by a system of three first order hyperbolic equations for the two velocity components and the pressure. Hence, the obvious advantage of the second order formulation is that the size of the system is reduced. Both continuous formulations need one boundary condition to form a well-posed initial-boundary value problem, which means that two extrapolation boundary conditions must be supplied to close the discretized first order system. This can be done, but one has to be careful not to introduce instabilities [3]. Furthermore, if the solution is not properly resolved

†Department of Mathematics, University of California, Los Angeles, Los Angeles, CA 90024 (kreiss@math.ucla.edu).

‡Center for Applied Scientific Computing, Lawrence Livermore National Laboratory, Livermore, CA 94551 (andersp@llnl.gov).
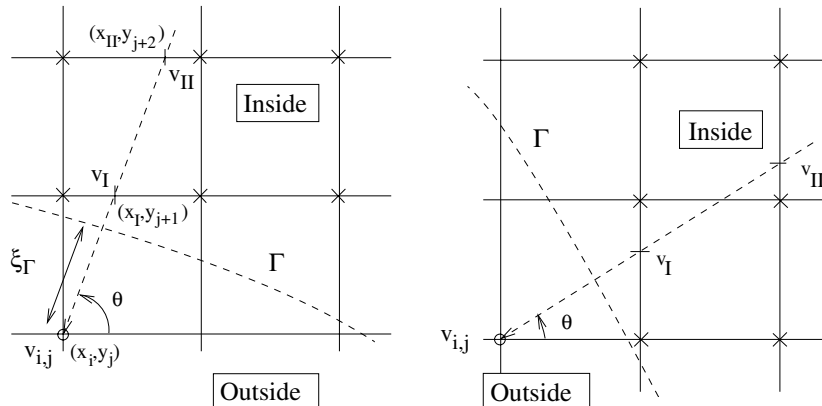
FIG. 1. *The points used for discretizing the Dirichlet boundary condition for the cases of horizontal interpolation (left) and vertical interpolation (right).*

on the grid, the discretized first order system allows for spurious waves that travel in the wrong direction [4]. The latter two problems can be circumvented by using a staggered grid (which amounts to nothing else but solving the original second order problem in disguise). However, when the boundary is not aligned with the grid, it is hard to find an accurate and stable staggered grid discretization of the boundary conditions. In contrast, the second order formulation does not need extrapolation boundary conditions and, as we have shown in [1], a node based discretization of the second order formulation avoids the difficulties with spurious waves traveling in the wrong direction. The subject of the present paper is to derive a stable second order accurate discretization of the wave equation subject to Dirichlet boundary conditions on boundaries that are not aligned with the grid.

A Cartesian embedded boundary approach will be used to solve the above problem numerically. We cover the domain Ω by a regular Cartesian grid with points $\boldsymbol{x}_{i,j} = (ih, jh)^T$, where i, j are integers and h is the grid size. The boundary is allowed to intersect the grid in an arbitrary manner; see Figure 1. Centered finite differences are used to discretize the wave equation in both space and time and the boundary condition is approximated using straightforward interpolation. However, the details of how the boundary condition is discretized are important since they determine the accuracy and stability of the numerical method. In the current paper, we discretize the Dirichlet boundary condition such that both the solution and its gradient become second order accurate. Furthermore, we add an artificial term to the discrete boundary condition that removes the stiffness due to small cells cut by the boundary without sacrificing the second order accuracy of the method. As a result, we can use an explicit time-integration method where the time step essentially equals that of a periodic domain. Stability of the method is obtained by using a small fourth order stabilizing term of the form $h^3 A^T A u_t$, where A is the matrix representation of the discrete Laplace operator satisfying the discrete boundary condition [2].

The embedded boundary technique for discretizing partial differential equations dates back to the first order technique by Weller and Shortley [5] and the higher order generalizations of Collatz [6]. More recently, several embedded boundary methods have been presented for various types of partial differential equations. For example, Pember et al. [7] used a Cartesian grid method for solving the time-dependent equa-

tions of gas dynamics. For the one- and two-dimensional Euler equations, Berger, Helzel, and LeVeque [8] developed a Cartesian "h-box" method which aims at avoiding the small-cell time step restriction without sacrificing accuracy. Zhang and LeVeque [9] solved the acoustic wave equation with discontinuous coefficients written as a first order system. A staggered grid method was used by Ditkowski, Dridi, and Hesthaven [10] for solving Maxwell's equations on a Cartesian grid. The methods described in these papers all solve first order systems (in time). For Poisson's equation with Dirichlet boundary conditions, Johansen and Colella [11] derived an embedded boundary technique based on the finite volume method combined with multigrid. More recently, Li and Greengard [12] developed a method for the scalar second order wave equation in two space dimensions, which combines a free-space Green's function evolution formula with an integral equation technique to satisfy Dirichlet or Neumann boundary conditions.

We have previously developed a Cartesian embedded boundary method for solving the wave equation subject to Dirichlet conditions [1]. That numerical method produces a solution that is second order accurate in max-norm, but the gradient of the solution is only first order accurate. Having accurate gradients is important in applications such as the elastic wave equation, where the stresses depend on the gradient of the displacement and the boundary condition on a free surface is expressed in terms of the stresses. As a step toward solving the elastic wave equation, we will here consider Maxwell's equations written as a second order wave equation for the electric field. In this application it is important to compute the gradient of the electric field to second order accuracy, since the time derivative of the magnetic field depends on the curl of the electric field.

There are two reasons why difference methods that use the embedded boundary discretization technique have problems calculating gradients with full accuracy:

1. Even if the initial data are fully compatible with the boundary condition for the analytic problem, the spatial discretization can destroy the compatibility on the truncation error level, which can degrade the rate of convergence for the gradient. This problem occurs already in one space dimension, and in section 2 we will discuss how it can be avoided by using a "smooth start" procedure, where we change variables

$$(5) \qquad\qquad u(\boldsymbol{x}, t) = \tilde{u}(\boldsymbol{x}, t) + (u_0(\boldsymbol{x}) + tu_1(\boldsymbol{x}))e^{-t^2}$$

   and numerically solve the problem for $\tilde{u}$. Since the new variable $\tilde{u}$ satisfies a modified wave equation subject to homogeneous initial conditions, there will be no incompatibilities on the truncation error level for the solution or its first time derivative.

2. Because the boundary is embedded in a regular Cartesian grid, the truncation error in the boundary condition can oscillate wildly between consecutive grid points along the boundary. This problem occurs in two or more space dimensions and can again degrade the rate of convergence for the gradient. In section 3, we first analyze this problem for Poisson's equation and then show that the wave equation behaves in the same way as long as the truncation error is smooth in time and compatible with the initial conditions. The analysis shows that due to the highly oscillatory truncation error, the Dirichlet boundary condition must be discretized using a third order accurate formula to obtain a second order accurate gradient of the solution. The analysis also shows that a second order truncation error that varies smoothly along the

boundary also results in a second order accurate gradient.

Guided by these results, we develop a new Cartesian embedded boundary method for the Dirichlet problem which we outline now. Let $v_{i,j}(t)$ denote the semidiscrete approximation of $u(x_i, y_j, t)$. A second order approximation of the Laplacian of u is given by

$$(6) \qquad \Delta_h v_{i,j} =: \frac{1}{h^2}(v_{i+1,j} + v_{i-1,j} + v_{i,j+1} + v_{i,j-1} - 4v_{i,j}).$$

To be able to evaluate $\Delta_h v_{i,j}$ at all grid points inside Ω, we use ghost points just outside the domain; see Figure 1. Let x_I, x_{II} be the intersections between the normal going through $\boldsymbol{x}_{i,j}$ and the grid lines $y = y_{j+1}$ and $y = y_{j+2}$, respectively. Denote by ξ_I, $\xi_{II} = 2\xi_I$ the distances between $\boldsymbol{x}_{i,j}$ and (x_I, y_{j+1}), (x_{II}, y_{j+2}), respectively. To aid in the approximation of the Dirichlet condition, we construct a Lagrange interpolant between three points along the normal: $(0, v_{i,j})$, (ξ_I, v_I), (ξ_{II}, v_{II}),

$$(7) \qquad Lv =: g_0(\xi_\Gamma)v_{i,j} + g_I(\xi_\Gamma)v_I + g_{II}(\xi_\Gamma)v_{II},$$

where the coefficients are given by

$$(8) \qquad g_0(\xi) = \frac{(\xi_I - \xi)(2\xi_I - \xi)}{2\xi_I^2}, \quad g_I(\xi) = \frac{\xi(2\xi_I - \xi)}{\xi_I^2}, \quad g_{II}(\xi) = \frac{\xi(\xi - \xi_I)}{2\xi_I^2}.$$

To approximate v_I and v_{II}, we interpolate along the horizontal grid lines y_{j+1} and y_{j+2}:

$$(9) \qquad v_I = d_1 v_{i,j+1} + d_2 v_{i+1,j+1} + d_3 v_{i+2,j+1},$$
$$(10) \qquad v_{II} = d_4 v_{i,j+2} + d_5 v_{i+1,j+2} + d_6 v_{i+2,j+2},$$

where $d_k = \mathcal{O}(1)$ are the quadratic Lagrange interpolation coefficients. The interpolant $Lu(t)$ is a third order approximation of the boundary value, i.e., $Lu(t) = u(\boldsymbol{x}_{i,j}^\Gamma, t) + \mathcal{O}(h^3)$, where $\boldsymbol{x}_{i,j}^\Gamma$ is the intersection point between the boundary and the normal going through the ghost point $\boldsymbol{x}_{i,j}$.

The interpolation formulas for v_I and v_{II}, (9)–(10), hold when the angle θ between the normal and the x-axis satisfies $\pi/4 \leq \theta \leq \pi/2$. When $0 \leq \theta \leq \pi/4$, the horizontal interpolations are replaced by corresponding interpolations in the vertical direction; see Figure 1. Despite the sudden switching between horizontal and vertical interpolation at $\theta = \pi/4$, the interpolation formulas for v_I and v_{II} are Lipschitz continuous in θ. Approaching the limit from above, the coefficients in the horizontal interpolation formulas (9)–(10) tend to $d_2 = d_6 = 1$, $d_1 = d_3 = d_4 = d_5 = 0$. Geometrically, this corresponds to the normal intersecting the mesh along the diagonal, so $v_I = v_{i+1,j+1}$ and $v_{II} = v_{i+2,j+2}$. The same limit is found with the corresponding vertical interpolation formulas as $\theta \to \pi/4$ from below. The Lipschitz continuity also holds at $\theta = \pi/2$, where the horizontal interpolation switches from using points to the right of the ghost point to using points to the left of it. At $\theta = \pi/2$, both the left and the right interpolation formulas use $v_I = v_{i,j+1}$ and $v_{II} = v_{i,j+2}$. The same argument shows Lipschitz continuity at $\theta = 0$, where the vertical interpolation switches from using points above the ghost point to using points below it. The formulas in the other three quadrants are simply obtained by reflections in index space, leading to a total of 8 different cases to treat all possible directions of the boundary.

When the normal is close to vertical (or horizontal), the boundary can intersect the grid such that ξ_Γ is arbitrarily close to ξ_I; i.e., $g_0(\xi_\Gamma)$ can be arbitrarily close to

zero. The limit $\xi_\Gamma = \xi_I$ corresponds to v_I being on the boundary and coinciding with a grid point, in which case one could eliminate the ghost point from the computation and simply use $v_I = f$ as a discrete boundary condition. This could be achieved for one ghost point by shifting the mesh appropriately. But for a general two-dimensional domain discretized on a fine grid, there can be thousands of ghost points and it is not possible to move the mesh to ensure that ξ_Γ stays bounded away from ξ_I for all ghost points simultaneously. Hence, it is important that the discretization of the boundary condition works for arbitrarily small $g_0(\xi_\Gamma)$.

If (7) were used to approximate the boundary condition, i.e., $Lv(t) = f(\boldsymbol{x}_{i,j}^\Gamma, t)$, we would need to divide by $g_0(\xi_\Gamma)$ to solve for the ghost point value using

$$(11) \qquad v_{i,j} = \frac{1}{g_0(\xi_\Gamma)} \left(f(\boldsymbol{x}_{i,j}^\Gamma, t) - g_I(\xi_\Gamma)v_I - g_{II}(\xi_\Gamma)v_{II} \right).$$

The ghost point value is used to evaluate the discrete Laplacian (6), and as we demonstrate for the one-dimensional case in Appendix A, (11) would make the time-stepping of (1) very stiff as $g_0 \to 0$. This phenomenon is known as the small-cell stiffness problem. To mitigate the stiffness, we add an artificial term to the interpolant (7) and instead consider

$$(12) \quad B_h v(t) =: g_0(\xi_\Gamma)v_{i,j} + g_I(\xi_\Gamma)v_I + g_{II}(\xi_\Gamma)v_{II} + \gamma(v_{i,j} - 2v_I + v_{II}) = f(\boldsymbol{x}_{i,j}^\Gamma, t),$$

where the constant $\gamma > 0$. The artificial term is an undivided second difference in the normal direction, and thus it inflicts an $\mathcal{O}(h^2)$ error in the boundary condition approximation. When the direction of the normal changes smoothly along the boundary, the error due to the artificial term also varies smoothly along the boundary. This is precisely the situation analyzed in section 3, since the truncation error in the boundary condition is composed of a highly oscillatory $\mathcal{O}(h^3)$ part and a smooth $\mathcal{O}(h^2)$ component. The accuracy of both the solution and its discrete gradient should therefore be $\mathcal{O}(h^2)$.

Because of the artificial term in the boundary condition, the coefficient in front of the ghost point $v_{i,j}$ is bounded uniformly away from zero, since

$$\gamma \le g_0(\xi_\Gamma) + \gamma < 1 + \gamma.$$

As a result, the small-cell stiffness problem is removed. By estimating the spectrum for the one-dimensional wave equation, we find that the eigenvalue with the largest magnitude is independent of small cells near the boundary when $\gamma \ge 0.25$; see Appendix A. Numerical computations indicate that $0.2 \le \gamma \le 0.5$ works well in practice; i.e., it is big enough to allow the time step to be chosen independently of the small cells near the boundary but small enough to prevent the artificial term from dominating the error in the numerical solution.

We can use the boundary condition (12) to eliminate all ghost points in the discrete Laplacian (6). For example, at the point $(i, j+1)$ in the left part of Figure 1 we get

$$(13) \quad \Delta_h v_{i,j+1} = \frac{1}{h^2}(v_{i+1,j+1} + v_{i-1,j+1} + v_{i,j+2} - 4v_{i,j+1})$$
$$- \frac{(g_I - 2\gamma)}{h^2(g_0 + \gamma)}(d_1 v_{i,j+1} + d_2 v_{i+1,j+1} + d_3 v_{i+2,j+1})$$
$$- \frac{(g_{II} + \gamma)}{h^2(g_0 + \gamma)}(d_4 v_{i,j+2} + d_5 v_{i+1,j+2} + d_6 v_{i+2,j+2}) + \frac{f(\boldsymbol{x}_{i,j}^\Gamma, t)}{h^2(g_0 + \gamma)},$$

assuming that (i, j) is the only nearest neighbor of $(i, j + 1)$ that is outside of Ω. (If additional points are outside, other formulas of the type (12) would be used to eliminate those points as well.) The expression (13) defines the discrete boundary forcing function $\boldsymbol{b}$ at point $(i, j + 1)$:

$$(14) \qquad\qquad \boldsymbol{b}_{i,j+1}(t) = \frac{f(\boldsymbol{x}_{i,j}^{\Gamma}, t)}{h^2(g_0 + \gamma)}.$$

In the interior of Ω, i.e., for points $\boldsymbol{x}_{i,j}$ where $\boldsymbol{x}_{i\pm1,j}$ and $\boldsymbol{x}_{i,j\pm1}$ are all inside Ω, $\boldsymbol{b}_{i,j}^n = 0$.

After all ghost points have been eliminated, the discrete approximation of the Laplacian of u (for functions satisfying the boundary condition $u = f(\boldsymbol{x}^{\Gamma}, t)$) can be written in matrix form

$$(15) \qquad\qquad \Delta u(\boldsymbol{x}, t) \approx A\boldsymbol{v}(t) + \boldsymbol{b}(t).$$

Here the array $\boldsymbol{v}$ contains the solution at all grid points inside Ω. Using this notation, the semidiscrete approximation of (1)–(4) becomes

$$(16) \qquad\qquad \boldsymbol{v}_{tt} = A\boldsymbol{v} + \boldsymbol{b}(t) + \boldsymbol{F}(t), \quad t \geq 0,$$
$$(17) \qquad\qquad \boldsymbol{v}(0) = u_0(\boldsymbol{x}), \qquad\qquad \boldsymbol{x} \in \Omega,$$
$$(18) \qquad\qquad \boldsymbol{v}_t(0) = u_1(\boldsymbol{x}), \qquad\qquad \boldsymbol{x} \in \Omega,$$

where $\boldsymbol{F}_{i,j}(t) = F(\boldsymbol{x}_{i,j}, t)$ for all $\boldsymbol{x}_{i,j} \in \Omega$.

We discretize the second order time derivative in (16) using a centered finite difference formula on the regular grid $t_n = nk$, $n = 0, 1, 2, \ldots$, where $k > 0$ is the time step. Let $\boldsymbol{v}^n = \boldsymbol{v}(t_n)$ and $\boldsymbol{b}^n = \boldsymbol{b}(t_n)$. Because of the discretized form of the Dirichlet boundary condition, the matrix A in (16) will not be symmetric. To avoid the resulting mild instability which was analyzed for the Neumann problem in [2], we use the discrete stabilization operator $h^3 A^T [A(\boldsymbol{v}^n - \boldsymbol{v}^{n-1})/k + d\boldsymbol{b}/dt(t_n)]$, which was proposed in the same paper. Note the time derivative of the boundary forcing is included within the brackets to make that expression a consistent approximation of Δu_t, for functions satisfying the boundary condition $u_t = f_t(\boldsymbol{x}^{\Gamma}, t)$. Also note that the discrete stabilization operator can be applied all the way up to the boundary. Away from the boundary, it is equivalent to $h^3 \Delta_h^2 (\boldsymbol{v}^n - \boldsymbol{v}^{n-1})/k$, which is a very efficient damping term for highly oscillatory instabilities. For the case with inhomogeneous boundary conditions and internal forcing, the proposed scheme becomes

$$(19)$$
$$\frac{\boldsymbol{v}^{n+1} - 2\boldsymbol{v}^n + \boldsymbol{v}^{n-1}}{k^2} = A\boldsymbol{v}^n + \boldsymbol{b}^n + \boldsymbol{F}(t_n) - \alpha h^3 A^T \left((A\boldsymbol{v}^n - A\boldsymbol{v}^{n-1})/k + \frac{d\boldsymbol{b}}{dt}(t_n) \right).$$

The numerical experiments in section 4 indicate that $\alpha = \mathcal{O}(10^{-3})$ suffices to stabilize the scheme for long time computations. We note that the sparse structure of A can be used to efficiently evaluate both $A\boldsymbol{v}$ and $A^T\boldsymbol{v}$ without the need to store the matrix explicitly; see [2]. Also note that this scheme bears many similarities with our method for the Neumann problem [2]. In particular, both methods use the same set of grid points for discretizing the boundary condition and the same type of stabilization term. Hence, the two methods can be combined in a straightforward manner to solve problems with mixed Neumann–Dirichlet conditions.

The remainder of the paper is organized as follows. The influence of incompatibilities between initial and boundary data on the truncation error level is analyzed in section 2 and the effect of highly oscillatory truncation errors in the boundary condition is studied in section 3. Two-dimensional numerical experiments are performed in section 4. We first construct a smooth solution against which the error in the numerical solution can be evaluated. The accuracy of the scheme and effects of the smooth start technique are evaluated in section 4.1. In section 4.2 we test the method by solving the TM_z problem for Maxwell's equations, i.e., the case when the electric field only has a component in the z-direction and the magnetic field has no component in the z-direction. The TM_z problem can be formulated as a scalar wave equation for the electric field in the (x, y) plane, subject to a Dirichlet boundary condition. The wave equation for the electric field is coupled to ODEs for the magnetic field that are integrated in time as the electric field is evolved. This is a good test of the scheme, since the accuracy of the magnetic field is determined by the accuracy of the curl of the electric field. Numerical experiments are performed for a circular domain where the numerical solution is compared to an analytic solution, as well as for more complex domains. Concluding remarks are presented in section 5.

2. Smooth start. We start by considering the one-dimensional half-plane problem

$$(20) \qquad u_{tt} = u_{xx} + F(x, t), \quad a \le x < \infty, \quad t \ge 0,$$

with initial data

$$(21) \qquad u(x, 0) = u_0(x), \quad u_t(x, 0) = u_1(x)$$

and the boundary condition

$$(22) \qquad u(a, t) = f(t).$$

We henceforth assume that all data belong to C^∞. Therefore also the solution is smooth, provided compatibility conditions are satisfied. In the one-dimensional setting, these are

$$
\begin{aligned}
u(a, 0) &= u_0(a) = f(0), \\
u_t(a, 0) &= u_1(a) = f_t(0), \\
u_{tt}(a, 0) &= u_{0xx}(a) + F(a, 0) = f_{tt}(0), \\
(23) \qquad u_{ttt}(a, 0) &= u_{1xx}(a) + F_t(a, 0) = f_{ttt}(0), \\
u_{tttt}(a, 0) &= u_{0xxxx}(a) + F_{xx}(a, 0) + F_{tt}(a, 0) = f_{tttt}(0), \\
u_{ttttt}(a, 0) &= u_{1xxxx}(a) + F_{xxt}(a, 0) + F_{ttt}(a, 0) = f_{ttttt}(0), \\
&\vdots
\end{aligned}
$$

We introduce a grid

$$(24) \qquad x_\nu = \nu h, \quad \nu = 0, 1, 2, \ldots,$$

where $h > 0$ is the grid size. When the boundary is aligned with the grid, e.g., $a = 0$, a second order centered finite difference approximation of (20)–(22) yields the expected second order convergence of the numerical solution and its gradient. However, we are

interested in the case when the boundary is not aligned with the grid. We therefore take $a = (1 - \beta)h$, $0 < \beta < 1$, so that the boundary falls between x_0 and x_1. Hence, the grid point x_0 is outside the domain but will be used as a ghost point to aid in the difference approximation. Let $v(x_j, t)$ be a grid function approximating $u(x_j, t)$. The one-dimensional counterpart of the boundary condition (12) is

$$(25) \quad B_h^{(1)} v(t) =: c_0(\beta) v(x_0, t) + c_1(\beta) v(x_1, t) + c_2(\beta) v(x_2, t)$$
$$+ \gamma(v(x_0, t) - 2v(x_1, t) + v(x_2, t)) = f(t), \quad \gamma > 0,$$

where the coefficients satisfy

$$(26) \qquad c_0(\beta) = \frac{1}{2}\beta(1 + \beta), \quad c_1(\beta) = (1 - \beta)(1 + \beta), \quad c_2(\beta) = -\frac{1}{2}\beta(1 - \beta).$$

Similar to the two-dimensional case, we remove the stiffness in the time integration by taking $\gamma > 0$ such that the coefficient in front of $v(x_0, t)$ is bounded away from zero for $0 \leq \beta \leq 1$.

The semidiscrete difference approximation of (20)–(22) when the boundary is not aligned with the grid becomes

$$(27) \qquad v_{tt}(x_\nu, t) = D_+^x D_-^x v(x_\nu, t) + F(x_\nu, t), \quad \nu = 1, 2, \dots,$$
$$(28) \qquad v(x_\nu, 0) = u_0(x_\nu), \quad v_t(x_\nu, 0) = u_1(x_\nu), \quad \nu = 1, 2, \dots,$$
$$(29) \qquad B_h^{(1)} v(t) = f(t),$$

where $D_+^x v(x_\nu, t) = (v(x_{\nu+1}, t) - v(x_\nu, t))/h$ is the usual forward divided difference operator in the x-direction and $D_-^x v(x_\nu, t) = D_+^x v(x_{\nu-1}, t)$. For later use, we also define the centered operator $D_0^x v(x_\nu, t) = (v(x_{\nu+1}, t) - v(x_{\nu-1}, t))/(2h)$. Using Taylor series expansions, we see that the error $e(x_\nu, t) = u(x_\nu, t) - v(x_\nu, t)$ satisfies

$$(30) \qquad e_{tt}(x_\nu, t) = D_+^x D_-^x e(x_\nu, t) - \frac{h^2}{12} u_{xxxx}(x_\nu, t) + \mathcal{O}(h^4), \quad \nu = 1, 2, \dots,$$
$$(31) \qquad e(x_\nu, 0) = e_t(x_\nu, 0) = 0, \quad \nu = 1, 2, \dots,$$
$$(32) \qquad B_h^{(1)} e(t) = \gamma h^2 u_{xx}(a, t) + h^3(C + \gamma\beta)u_{xxx}(a, t) + \mathcal{O}(h^4).$$

Since the data are $\mathcal{O}(h^2)$, $|e(\cdot, t)|_\infty = \mathcal{O}(h^2)$. To derive an estimate for the gradient of e, we first derive an equation for $w = e_{tt}$. By taking two time derivatives of the differential equation (30) and the boundary condition (32), we get

$$w_{tt}(x_\nu, t) = D_+^x D_-^x w(x_\nu, t) - \frac{h^2}{12} u_{xxxxtt}(x_\nu, t) + \mathcal{O}(h^4), \quad \nu = 1, 2, \dots,$$
$$B_h^{(1)} w(t) = \gamma h^2 u_{xxtt}(a, t) + h^3(C + \gamma\beta)u_{xxxtt}(a, t) + \mathcal{O}(h^4).$$

To derive initial data for w, we can apply the differential equation (30) to the initial data (31). However, this only applies away from the boundary. For $\nu \geq 2$ we have

$$w(x_\nu, 0) = -\frac{h^2}{12} u_{xxxx}(x_\nu, 0) + \mathcal{O}(h^4), \quad \nu = 2, 3, \dots,$$
$$w_t(x_\nu, 0) = -\frac{h^2}{12} u_{xxxxt}(x_\nu, 0) + \mathcal{O}(h^4), \quad \nu = 2, 3, \dots.$$

To evaluate the initial data at the first interior point x_1, we must first apply the boundary condition (32) to define $e(x_0, 0)$:

$$B_h^{(1)} e(0) =: (c_0 + \gamma)e(x_0, 0) + (c_1 - 2\gamma)e(x_1, 0) + (c_2 + \gamma)e(x_2, 0)$$
$$= \gamma h^2 u_{xx}(a, 0) + h^3(C + \gamma\beta)u_{xxx}(a, 0) + \mathcal{O}(h^4).$$

Since $e(x_1, 0) = e(x_2, 0) = 0$, $D_+^x D_-^x e(x_1, 0) = e(x_0, 0)/h^2$. Therefore, (30) gives us

$$w(x_1, 0) = e_{tt}(x_1, 0) = \frac{\gamma}{c_0 + \gamma}u_{xx}(a, 0) + \frac{h(C + \gamma\beta)}{c_0 + \gamma}u_{xxx}(a, 0) + \mathcal{O}(h^2).$$

By taking the time derivative of the boundary condition, the same procedure can be used to obtain

$$w_t(x_1, 0) = e_{ttt}(x_1, 0) = \frac{\gamma}{c_0 + \gamma}u_{xxt}(a, 0) + \frac{h(C + \gamma\beta)}{c_0 + \gamma}u_{xxxt}(a, 0) + \mathcal{O}(h^2).$$

Hence, in general the forcing in the initial data is $\mathcal{O}(1)$ at the first interior point, which makes $|w(\cdot, t)|_\infty = \mathcal{O}(1)$. Consequently, $|D_+^x D_-^x e(\cdot, t)|_\infty = \mathcal{O}(1)$ and we can not obtain the desired estimate for the gradient of e.

The situation is much better in the case with homogeneous initial data, $u_0(x) = u_1(x) = 0$. Now all spatial derivatives of u and u_t are initially zero, so the initial data for w are

$$w(x_\nu, 0) = w_t(x_\nu, 0) = 0, \quad \nu = 1, 2, \dots.$$

Hence the forcing for w is $\mathcal{O}(h^2)$. Therefore, we can derive an estimate for $|e_{tt}(\cdot, t)|_\infty = |w(\cdot, t)|_\infty = \mathcal{O}(h^2)$ and

$$|D_+^x D_-^x e(\cdot, t)|_\infty \le |w(\cdot, t)|_\infty + \frac{h^2}{12}|u_{xxxx}(\cdot, t)|_\infty = \mathcal{O}(h^2).$$

Since $|D_+^x e(\cdot, t)|_\infty$ can be estimated in terms of e and $D_+^x D_-^x e$ using a discrete Sobolev inequality (see, e.g., [13]), we have

$$|D_+^x e|_\infty = \mathcal{O}(h^2).$$

A problem with general, but compatible, initial data can be reformulated into a problem with homogeneous initial data by changing variables according to (5). If the original variable u satisfies (1)–(4), the variable $\tilde{u}$ satisfies the modified problem

$$\begin{align}
\tilde{u}_{tt} &= \Delta\tilde{u} + \tilde{F}(\boldsymbol{x}, t), & \boldsymbol{x} \in \Omega, \quad t \ge 0, \tag{33}\\
\tilde{u}(\boldsymbol{x}, t) &= \tilde{f}(\boldsymbol{x}, t), & \boldsymbol{x} \in \Gamma, \quad t \ge 0, \tag{34}\\
\tilde{u}(\boldsymbol{x}, 0) &= 0, & \boldsymbol{x} \in \Omega, \tag{35}\\
\tilde{u}_t(\boldsymbol{x}, 0) &= 0, & \boldsymbol{x} \in \Omega, \tag{36}
\end{align}$$

where the modified internal forcing function is

$$\tilde{F}(\boldsymbol{x}, t) = F(\boldsymbol{x}, t) + \left[\Delta u_0(\boldsymbol{x}) + t\Delta u_1(\boldsymbol{x}) + (2 - 4t^2)u_0(\boldsymbol{x}) + (6t - 4t^3)u_1(\boldsymbol{x})\right]e^{-t^2}$$

and the boundary forcing becomes

$$\tilde{f}(\boldsymbol{x}, t) = f(\boldsymbol{x}, t) - [u_0(\boldsymbol{x}) + tu_1(\boldsymbol{x})]e^{-t^2}, \quad \boldsymbol{x} \in \Gamma.$$

To solve the problem for $u(\boldsymbol{x}, t)$, we first compute $\tilde{u}(\boldsymbol{x}, t)$ numerically and then add in $(u_0(\boldsymbol{x}) + tu_1(\boldsymbol{x}))e^{-t^2}$ to obtain the solution of the original problem. By doing so, we obtain a second order accurate solution where the gradient and second derivative of the numerical solution are also second order accurate.

To verify the above theory, we solve the embedded boundary problem (27)–(29) numerically. Now we consider the bounded domain

$$a \leq x \leq b$$

and add a boundary condition at $x = b$,

$$u(b, t) = f_2(t).$$

The interior grid points are $q_0 \leq \nu \leq q_1$ such that $a + \beta h = x_{q_0}$ and $x_{q_1} + \beta_2 h = b$, $0 < \beta_2 < 1$. We take initial data, interior forcing function, and boundary forcing functions such that the analytic problem is solved by $u(x, t) = \sin(2x - t + \pi/4)$, i.e.,

$$
\begin{aligned}
F(x_\nu, t) &= 3\sin(2x_\nu - t + \pi/4), \\
f(t) &= \sin(2a - t + \pi/4), \\
f_2(t) &= \sin(2b - t + \pi/4), \\
u_0(x_\nu) &= \sin(2x_\nu + \pi/4), \quad u_1(x_\nu) = -\cos(2x_\nu + \pi/4).
\end{aligned}
$$

We introduce a grid in time $t_n = nk$, $k > 0$ and discretize time derivatives by centered differences. We set $h = 2\pi/N$, where N is a positive integer, so that $x_N = 2\pi$. The boundary condition at $x = a$ is discretized by (25), shifted to involve the points $(q_0 - 1, q_0, q_0 + 1)$. The boundary condition at $x = b$ is discretized using a corresponding formula involving the points $(q_1 - 1, q_1, q_1 + 1)$ with β_2 replacing β. We arrive at the following explicit time integration scheme:

$$
\begin{aligned}
D_+^t D_-^t v(x_\nu, t_n) &= D_+^x D_-^x v(x_\nu, t_n) + F(x_\nu, t_n), \quad \nu = q_0, q_0 + 1, \ldots, q_1, \\
v(x_\nu, 0) &= u_0(x_\nu), \quad \nu = q_0, q_0 + 1, \ldots, q_1,
\end{aligned}
$$

$$
\text{(37)} \qquad v(x_\nu, -k) = u_0(x_\nu) - ku_1(x_\nu) + \frac{k^2}{2}\left(u_{0xx}(x_\nu, 0) + F(x_\nu, 0)\right)
$$

$$
- \frac{k^3}{6}\left(u_{1xx}(x_\nu, 0) + F_t(x_\nu, 0)\right), \quad \nu = q_0, q_0 + 1, \ldots, q_1,
$$

$$
B_h^{(a)} v(t_n) = f(t_n), \quad B_h^{(b)} v(t_n) = f_2(t_n).
$$

One can show that the above scheme is stable for $k/h < 1$ when $\gamma \geq 0.25$; see [1] and Appendix A. Numerical computations (see Table 1) indicate that the solution is second order accurate, but the gradient is only a little better than first order accurate and the second derivative has an $\mathcal{O}(1)$ error. However, by using the smooth start procedure, i.e., changing variables according to (5) and numerically solving (33)–(36), second order accuracy is also obtained for the gradient and the second derivative; see Table 2.

We have also observed that the convergence of the gradient improves when the initial data is inhomogeneous, but the interior and boundary forcing functions are homogeneous, $F(x, t) = 0$, $f(t) = 0$. From the compatibility relations (23), we see that all even spatial derivatives of u and u_t are zero at $x = a$, $t = 0$. In particular, $u_{xx}(a, 0) = 0$ and $u_{xxt}(a, 0) = 0$, so the leading order terms in the initial data for w become one order smaller in h. Hence, $w(x_1, 0) = \mathcal{O}(h)$ and $w_t(x_1, 0) = \mathcal{O}(h)$,

TABLE 1
Direct start: Error in the computed solution when the boundary is embedded between grid points. The errors are reported at time $t = 6.333$, the domain is $0.37 \leq x \leq 5.1$, $\gamma = 0.2$, and $k/h = 0.9$.

N	$\|u - v\|_\infty$	$\|\frac{\partial u}{\partial x} - D_0^x v\|_\infty$	$\|\frac{\partial^2 u}{\partial x^2} - D_+^x D_-^x v\|_\infty$	β	β_2
200	1.22×10^{-3}	9.36×10^{-3}	1.88×10^0	0.222	0.338
400	2.53×10^{-4}	3.13×10^{-3}	3.59×10^{-1}	0.445	0.676
800	6.29×10^{-5}	1.26×10^{-3}	2.98×10^{-1}	0.890	0.352

TABLE 2
Smooth start: Error in the computed solution when the boundary is embedded between grid points. The errors are reported at time $t = 6.333$, the domain is $0.37 \leq x \leq 5.1$, $\gamma = 0.2$, and $k/h = 0.9$.

N	$\|u - v\|_\infty$	$\|\frac{\partial u}{\partial x} - D_0^x v\|_\infty$	$\|\frac{\partial^2 u}{\partial x^2} - D_+^x D_-^x v\|_\infty$	β	β_2
200	8.90×10^{-4}	1.14×10^{-3}	1.02×10^{-3}	0.222	0.338
400	2.22×10^{-4}	2.86×10^{-4}	2.56×10^{-4}	0.445	0.676
800	5.55×10^{-5}	7.09×10^{-5}	6.38×10^{-5}	0.890	0.352

and we get $|w(\cdot, t)|_\infty = \mathcal{O}(h)$. Hence, $|e(\cdot, t)|_\infty = \mathcal{O}(h^2)$ but $|D_+^x D_-^x e(\cdot, t)|_\infty = \mathcal{O}(h)$. Numerical experiments suggest that the solution and its gradient are second order accurate but the second derivative is only first order accurate. Naturally, the error in the second derivative can be made second order accurate also in this case by using smooth start.

There are also cases when the smooth start procedure is not necessary. This occurs, for example, when the boundary data are homogeneous, $f(t) = 0$, and the internal forcing and initial data have compact support in the interior of Ω.

3. An analytic model of the Dirichlet problem. In this section we first consider Poisson's equation

$$(38) \qquad u_{xx} + u_{yy} = F(x, y)$$

on the half-plane $y - 2x \leq 0$ with Dirichlet boundary conditions

$$(39) \qquad u(x, y) = f(x, y) \quad \text{for} \quad y = 2x.$$

We want to solve the problem numerically, use the same Cartesian grid as before, and approximate (38) by the second order approximation

$$\Delta_h v(x_m, y_l) = F_h(x_m, y_l)$$

in all interior points. Here F_h is the restriction of F to the grid.

The grid is not aligned with the boundary. Along the boundary only every second point is on the grid. A second order accurate approximation of (39) is, for example, given by

$$(40) \qquad v(lh, 2lh) = f(lh, 2lh),$$

$$(41) \quad \frac{1}{2}\left\{v\big((l-1)h, (2l-1)h\big) + v\big(lh, (2l-1)h\big)\right\} = f\left(\left(l - \frac{1}{2}\right)h, (2l-1)h\right)$$

for $l = 0, \pm 1, \pm 2, \ldots$. We write (40)–(41) formally as

$$B_h v = f_h.$$

To obtain an error estimate we assume that the solution of (38)–(39) is smooth. (This is, for example, the case if F, f are smooth and decay rapidly as $|x| + |y| \to \infty$; cf. [14].) The usual truncation error analysis gives us, for the error $e = v - u$ on the grid,

(42) $$\Delta_h e = h^2 G \quad \text{in the interior,}$$
(43) $$B_h e = h^2 g \quad \text{on the boundary.}$$

Here G is the restriction of a smooth function to the grid but g is, in general, not smooth. The boundary condition (41) implies that g oscillates between 0 and $u_{xx} + \mathcal{O}(h^2)$ from grid point to grid point. This rapid change is typical for embedded boundary difference approximations in general domains.

If we want only to estimate e, this is tolerable because one can prove, using the discrete maximum principle, that the error is $\mathcal{O}(h^2)$. However, if we also want to calculate the gradient, then the error degrades, in general, to $\mathcal{O}(h)$. This degradation does not depend on G. If $G \neq 0$, we solve an auxiliary problem

(44) $$\Delta_h e_1 = h^2 G \quad \text{in the interior,}$$
(45) $$B_h e_1 = 0 \quad \text{on the boundary.}$$

The problem (44)–(45) is a second order accurate approximation of

$$\Delta u_1 = h^2 G \quad \text{in the interior,}$$
$$u_1 = 0 \quad \text{on the boundary.}$$

The function u_1 and its gradient are of order $\mathcal{O}(h^2)$. Since $e_1 - u_1 = \mathcal{O}(h^4)$ on the grid, the discrete gradient of e_1 is $\mathcal{O}(h^2)$. Subtracting the solution of (44)–(45) from the solution of (42)–(43) shows that we can assume that $G \equiv 0$; i.e., we discuss

(46) $$\Delta_h e = 0 \quad \text{in the interior,}$$
(47) $$B_h e = h^2 g \quad \text{on the boundary.}$$

To gain insight into the effects of highly oscillatory boundary data, we analyze a modified equation model of (46)–(47). A more sophisticated analysis, where the discrete nature of the problem is taken into account, will be presented elsewhere. The problem (46)–(47) is a second order accurate approximation of

(48) $$\Delta e = 0, \quad y - 2x \leq 0,$$
(49) $$e = h^2 g, \quad y = 2x,$$

and we proceed by studying the properties of its solution, in particular when g is highly oscillatory. To simplify the notation, we rotate the coordinate system and introduce the new independent variables

(50) $$\xi = (2x - y)/\sqrt{5},$$
(51) $$\eta = (x + 2y)/\sqrt{5}.$$

The boundary is aligned with $\xi = 0$ and we consider the half-plane problem for $\xi \geq 0$. We assume that all functions are 2π-periodic in η. Fourier transforming (48)–(49) in η gives us

$$\hat{e}_{\xi\xi} - \omega^2 \hat{e} = 0, \quad \omega \text{ integer},$$
$$\hat{e}(0, \omega) = h^2 \hat{g}(\omega).$$

Since we are mainly interested in highly oscillatory g, we always assume that $\hat{g}(0) = 0$. Then the unique solution in L_2 is given by

$$(52) \qquad e = h^2 \sum_{\omega \neq 0} e^{-|\omega|\xi + i\omega\eta} \hat{g}(\omega),$$

and we have

$$e_\xi = -h^2 \sum_{\omega \neq 0} |\omega| e^{-|\omega|\xi + i\omega\eta} \hat{g}(\omega).$$

We make the following observations:

(1) If the boundary data are smooth, i.e., $\hat{g}(\omega)$ decays rapidly, then the solution is also smooth up to the boundary.

(2) If we only know that $g \in L_2$, then we obtain, for every fixed ξ,

$$\|e_\xi(\xi, \cdot)\|^2 = \int_{-\pi}^{\pi} |e_\xi(\xi, \eta)|^2 d\eta = \sum_{\omega \neq 0} |\omega|^2 e^{-2|\omega|\xi} |h^2 \hat{g}(\omega)|^2$$

$$= \frac{1}{\xi^2} \sum_{\omega \neq 0} |\xi\omega|^2 e^{-2|\omega|\xi} |h^2 \hat{g}(\omega)|^2 \leq \frac{\text{const.}}{\xi^2} \sum_{\omega \neq 0} e^{-|\omega|\xi} |h^2 \hat{g}(\omega)|^2.$$

Thus the solution becomes smooth away from the boundary layer at $\xi = 0$.

(3) If the boundary data are highly oscillatory, i.e.,

$$g(\eta) = \sum_{|\omega| \geq 1/h} e^{i\omega\eta} \hat{g}(\omega), \quad 0 < h \ll 1,$$

we obtain

$$\|e_\xi(\xi, \cdot)\|^2 \leq \frac{\text{const.}}{\xi^2} \sum_{|\omega| \geq 1/h} e^{-|\omega|\xi} |h^2 \hat{g}(\omega)|^2$$

$$\leq \frac{\text{const.}}{\xi^2} e^{-\xi/h} \sum_{|\omega| \geq 1/h} e^{-(|\omega| - 1/h)\xi} |h^2 \hat{g}(\omega)|^2;$$

i.e., the thickness of the boundary layer is $\mathcal{O}(h)$.

(4) The highest frequency on a grid is $|\omega h| = \pi$. Hence, if $\hat{g}(\omega) = 0$ for $|\omega| > \pi/h$, then

$$\|e_\xi(\xi, \cdot)\|^2 = \frac{1}{h^2} \sum_{|\omega h| \leq \pi} |\omega h|^2 e^{-2|\omega|\xi} |h^2 \hat{g}(\omega)|^2 \leq \pi^2 \sum_{|\omega h| \leq \pi} e^{-2|\omega|\xi} |h\hat{g}(\omega)|^2.$$

Thus the gradient is of the order $\mathcal{O}(h)$.

We would like to point out that these estimates correspond to Schauder-type interior regularity estimates; see, e.g., Chapters 4 and 6 of [14].

To summarize our results for the Dirichlet problem for Poisson's equation, the gradient is only of the order $\mathcal{O}(h^2)$ if the boundary data $h^2 g(\eta)$ are the restriction of a smooth function. For highly oscillatory $g(\eta)$, the gradient will be $\mathcal{O}(h)$. We can also use a third order accurate approximation of the boundary condition. Then the solution is of the order $\mathcal{O}(h^3)$ and the discrete gradient is of the order $\mathcal{O}(h^2)$, even if the boundary data are highly oscillatory. Since the problem is linear, we also get a discrete gradient of the order $\mathcal{O}(h^2)$ when the boundary data consist of a smooth $\mathcal{O}(h^2)$ term together with a highly oscillatory $\mathcal{O}(h^3)$ component.

3.1. The wave equation. We next consider the wave equation (1)–(4) on the half-plane $y - 2x \leq 0$. We use the same grid and the same spatial discretization as for Poisson's equation, and study the following semidiscrete approximation:

$$
\begin{aligned}
v_{tt}(x_m, y_l, t) &= \Delta_h v(x_m, y_l, t) + F_h(x_m, y_l, t), & y_l - 2x_m &< 0, \ t \geq 0, \\
B_h v(t) &= f_h(t) & \text{on the boundary}, \ t &\geq 0, \\
v(x_m, y_l, 0) &= u_0(x_m, y_l), & y_l - 2x_m &< 0, \\
v_t(x_m, y_l, 0) &= u_1(x_m, y_l), & y_l - 2x_m &< 0.
\end{aligned}
$$

Again we are interested in the accuracy of the solution and its gradient. We assume that F, u_0, and u_1 are smooth functions that can be expanded smoothly to the entire plane such that they decay rapidly as $|x| + |y| \to \infty$. Therefore, we can assume that

$$(53) \qquad\qquad F \equiv u_0 \equiv u_1 \equiv 0.$$

Otherwise, we would first solve the continuous and semidiscrete Cauchy problems which we would then subtract from u and v, respectively. The gradient of the solution of the semidiscrete Cauchy problem has full accuracy since it satisfies the same equation as the solution itself (with different data). Thus we consider

$$
\begin{aligned}
u_{tt} &= \Delta u, & y - 2x &\leq 0, & t &\geq 0, \\
u(x, y, t) &= f(x, y, t), & y - 2x &= 0, & t &\geq 0, \\
u(x, y, 0) &= u_t(x, y, 0) = 0, & y - 2x &\leq 0.
\end{aligned}
$$

If $f(x, 2x, 0) \neq 0$, then the boundary data are not compatible with the initial data. If we want the solution to have p bounded time derivatives, we need

$$(54) \qquad \partial^j f(x, y, t)/\partial t^j \big|_{t=0} = 0, \quad j = 0, 1, 2, \ldots, p - 1, \quad y = 2x.$$

The corresponding difference approximation is

$$
\begin{aligned}
v_{tt}(x_m, y_l, t) &= \Delta_h v(x_m, y_l, t), & y_l - 2x_m &< 0, \ t \geq 0, \\
B_h v(t) &= f_h(t) & \text{on the boundary}, \ t &\geq 0, \\
v(x_m, y_l, 0) &= v_t(x_m, y_l, 0) = 0, & y_l - 2x_m &< 0.
\end{aligned}
$$

We want to obtain an estimate for the error $e = v - u$ on the grid, and by using the same truncation error technique as for Poisson's equation, we get the following discrete error equation:

$$
\begin{aligned}
e_{tt}(x_m, y_l, t) &= \Delta_h e(x_m, y_l, t), & y_l - 2x_m &< 0, \ t \geq 0, \\
B_h e(t) &= h^2 g_h(t) & \text{on the boundary}, \ t &\geq 0, \\
e(x_m, y_l, 0) &= e_t(x_m, y_l, 0) = 0, & y_l - 2x_m &< 0,
\end{aligned}
$$

where g_h is highly oscillatory in space but smooth in time (because the interpolation formulas do not depend on time). We proceed as for Poisson's equation and study the continuous modified equation model of the discrete error equation:

$$
\begin{aligned}
e_{tt} &= \Delta e, & y - 2x < 0,\ t \geq 0, \\
e &= h^2 g, & y - 2x = 0,\ t \geq 0, \\
e(x, y, 0) = e_t(x, y, 0) &= 0, & y - 2x < 0.
\end{aligned}
$$

By rotating the coordinate system according to (50)–(51), we align the boundary with $\xi = 0$ and arrive at a half-plane problem for $\xi \geq 0$, $-\infty < \eta < \infty$. Up to now, we have assumed a second order accurate discretization of the boundary condition, but the same arguments also apply to a higher order boundary discretization. We therefore take $\phi = h^2 g$ and study the half-plane problem

$$
\begin{aligned}
e_{tt} &= \Delta e, \\
e(0, \eta, t) &= \phi(\eta, t), \\
e(\xi, \eta, 0) = e_t(\xi, \eta, 0) &= 0.
\end{aligned}
\tag{55}
$$

We assume that all data are 2π-periodic functions in η, Fourier transform the problem in the η-direction, and obtain

$$
\begin{aligned}
\hat{e}_{tt} &= \hat{e}_{\xi\xi} - \omega^2 \hat{e}, \\
\hat{e}(0, \omega, t) &= \hat{\phi}(\omega, t), \\
\hat{e}(\xi, \omega, 0) = \hat{e}_t(\xi, \omega, 0) &= 0,
\end{aligned}
\tag{56}
$$

with

$$
\partial^j \hat{\phi}(\omega, t) / \partial t^j \big|_{t=0} = 0, \quad j = 0, 1, 2, \ldots, p - 1.
$$

Because of the compatibility assumption (54), the solution will be smooth in time. If the boundary data are smooth in η, i.e., the Fourier coefficients $\hat{\phi}(\omega, t)$ decay rapidly for large ω, the solution will also be smooth in space. However, as we have seen before, the truncation error in the boundary condition is highly oscillatory in space, and we proceed by studying large $|\omega|$.

When $|\omega| \gg 1$, we solve (56) by iteration. For $j = 1, 2, \ldots$, let

$$
\begin{aligned}
\hat{e}^{(j)}_{\xi\xi} - \omega^2 \hat{e}^{(j)} &= \hat{e}^{(j-1)}_{tt}, \\
\hat{e}^{(j)}(0, \omega, t) &= \hat{\phi}(\omega, t).
\end{aligned}
$$

We take $\hat{e}^{(0)} = 0$, so $\hat{e}^{(1)}$ satisfies

$$
\begin{aligned}
\hat{e}^{(1)}_{\xi\xi} - \omega^2 \hat{e}^{(1)} &= 0, \\
\hat{e}^{(1)}(0, \omega, t) &= \hat{\phi}(\omega, t).
\end{aligned}
$$

The only bounded solution is $\hat{e}^{(1)}(\xi, \omega, t) = \hat{\phi}(\omega, t) e^{-|\omega|\xi}$. The problem for $\hat{e}^{(2)}$ becomes

$$
\begin{aligned}
\hat{e}^{(2)}_{\xi\xi} - \omega^2 \hat{e}^{(2)} &= \hat{\phi}_{tt}(\omega, t) e^{-|\omega|\xi}, \\
\hat{e}^{(2)}(0, \omega, t) &= \hat{\phi}(\omega, t),
\end{aligned}
$$

which is solved by

$$\hat{e}^{(2)} = \hat{e}^{(1)} - \frac{1}{2\omega^2}\hat{\phi}_{tt}|\omega|\xi e^{-|\omega|\xi}.$$

Note that $\alpha e^{-\alpha} \leq$ const. for $\alpha \geq 0$. Hence, for $|\omega| \gg 1$ the solution of (56) is

$$\hat{e}(\xi,\omega,t) = \hat{\phi}e^{-|\omega|\xi} - \frac{1}{2\omega^2}\hat{\phi}_{tt}|\omega|\xi e^{-|\omega|\xi} + \mathcal{O}\left(\frac{1}{\omega^4}\right).$$

As long as ϕ_{tt} is of the same order as ϕ, the gradient satisfies

$$\hat{e}_\xi(\xi,\omega,t) = \hat{e}_\xi^{(1)}(\xi,\omega,t)\left(1 + \mathcal{O}\left(\frac{1}{\omega^2}\right)\right).$$

Therefore, the properties of the gradient of $\hat{e}$ can be reduced to the properties of $\hat{e}^{(1)}$, which was studied in the previous section. Hence, for boundary data $\phi(\xi,t)$ which are highly oscillatory in space but smooth in time, the gradient of e only becomes large in a boundary layer near $\xi = 0$, while the solution remains smooth in the interior of the domain. This means that if the boundary approximation is third order accurate with a highly oscillatory truncation error, i.e., $\phi = h^3 g$, the gradient of the solution will be third order accurate except near the boundary $\xi = 0$, where it will be second order accurate.

Note that the time-smoothness assumption is essential because ϕ_{tt} appears as forcing for $\hat{e}^{(2)}$ and the number of time derivatives in the forcing will increase by two for each iteration. However, this is not only a technicality due to our way of constructing the solution. The error in the solution is studied numerically in the next section, and it can clearly be seen that the error in the gradient becomes large throughout the domain when the truncation error is not smooth in time; cf. Figure 2. This illustrates a major difference in the behavior of hyperbolic and elliptic problems. For elliptic problems, a high frequency boundary error will lead to a solution error that is unsmooth only in a boundary layer. In contrast, for hyperbolic problems, a boundary error which is highly oscillatory in both space and time will make the solution error highly oscillatory throughout the domain. The unsmooth solution error will be confined to a boundary layer only if the boundary error is smooth in time.

4. Numerical experiments. In this section we numerically solve (1)–(4) with the scheme described above. We denote the CFL-number by CFL $\equiv k/h$. Note that for a two-dimensional periodic domain our time-integration scheme (19) is stable for CFL $\leq 1/\sqrt{2} \approx 0.71$. Also note that all errors reported below are measured in max-norm over all grid points inside Ω.

We start the time integration at $n = 0$ and take $v_{i,j}^0 = u_0(x_i, y_j)$. We need to use a fourth order accurate approximation of $u(x_i, y_j, -k)$ for $v_{i,j}^{-1}$. This is achieved by using the differential equation to approximate the second and third time derivatives,

(57)

$$\begin{aligned}
v_{i,j}^{-1} = {}& u_0(x_i, y_j) - ku_1(x_i, y_j) + \frac{k^2}{2}\left(D_+^x D_-^x + D_+^y D_-^y\right)u_0(x_i, y_j) + \frac{k^2}{2}F(\boldsymbol{x}_{i,j}, 0) \\
& - \frac{k^3}{6}\left(D_+^x D_-^x + D_+^y D_-^y\right)u_1(x_i, y_j) - \frac{k^3}{6}F_t(\boldsymbol{x}_{i,j}, 0).
\end{aligned}$$

Note that when the smooth start procedure is employed, the initial data are homogeneous, and thus the above formula simplifies to

$$\tilde{v}_{i,j}^{-1} = \frac{k^2}{2}\tilde{F}(\boldsymbol{x}_{i,j},0) - \frac{k^3}{6}\tilde{F}_t(\boldsymbol{x}_{i,j},0),$$

where the modified forcing initially satisfies

$$\tilde{F}(\boldsymbol{x},0) = F(\boldsymbol{x},0) + 2u_0(\boldsymbol{x}) + \Delta u_0(\boldsymbol{x}), \quad \tilde{F}_t(\boldsymbol{x},0) = F_t(\boldsymbol{x},0) + 6u_1(\boldsymbol{x}) + \Delta u_1(\boldsymbol{x}).$$

To use the smooth start procedure, we need to evaluate Δu_k, $k = 0, 1$, at all interior grid points. When $u_0(x, y)$ and $u_1(x, y)$ are complicated analytic expressions of x and y, an appealing alternative is to approximate Δu_k by finite differences. Numerical experiments indicate that a centered second or fourth order accurate difference approximation of Δu_k, $k = 0, 1$, can replace analytic expressions without any noticeable degradation of the computed solutions, as long as u_0 and u_1 are well resolved on the grid. However, to define all values in the five- or seven-point formula for the centered difference approximation of the Laplacian, this approach works only if u_0 and u_1 can be evaluated at all interior grid points as well as one or two grid points outside the boundary, respectively.

4.1. Trigonometric exact solution. To evaluate the accuracy of the method and the properties of the smooth start technique, we begin by considering the case when the exact solution is known. Given a smooth function $U(\boldsymbol{x}, t)$, this is accomplished by constructing balancing interior and boundary forcing functions $F(\boldsymbol{x}, t) = U_{tt}(\boldsymbol{x}, t) - \Delta U(\boldsymbol{x}, t)$ and $f(\boldsymbol{x}_\Gamma, t) = U(\boldsymbol{x}_\Gamma, t)$, respectively. The initial data are obtained by setting $u_0(\boldsymbol{x}) = U(\boldsymbol{x}, 0)$, $u_1(\boldsymbol{x}) = U_t(\boldsymbol{x}, 0)$. The continuous problem is then discretized and the error in the discrete solution can be obtained by taking the difference between the numerical and analytic solutions at each grid point.

We choose the exact solution to be the trigonometric traveling wave

$$(58) \qquad U(x, y, t) = \sin(\omega(x - t)) \sin(\omega y), \quad \omega = 2\pi.$$

The domain Ω is taken to be an ellipse centered at the origin with semiaxes $x_s = 1$ and $y_s = 0.75$. The Cartesian grid covers the rectangle $-1.04 \le x \le 1.04$, $-0.78 \le y \le 0.78$, the grid size is $h = 2.08/(N - 1)$, and CFL = 0.5. To assess the accuracy of the scheme we run the computations until time $t = 2.0$. Note that no damping is necessary for these short runs ($\alpha = 0$). In Table 3, we present a grid refinement study for the scheme (19) started directly (from inhomogeneous initial data) and smoothly, respectively. In both cases, the solution itself converges as $\mathcal{O}(h^2)$, but the gradient and Laplacian are second order accurate only when smooth start is being used. (The second order formulas $D_0^x v_{i,j}$ and $D_0^y v_{i,j}$ are used to approximate the discrete gradient, and the component of the gradient with the largest error is reported. The Laplacian is approximated by $\Delta_h v_{i,j}$.) Note that when the computation is started directly, the error in the gradient is only a little better than first order accurate and the error in the Laplacian is $\mathcal{O}(1)$. This agrees with our observations for the one-dimensional case; cf. Table 1.

To more clearly see the impact of the smooth start procedure on the solution, in Figure 2 we plot the error in the solution at time $t = 2.0$, with direct and smooth start. Clearly, the smooth start procedure efficiently removes the high frequency errors present in the computation using direct start.

TABLE 3
Grid refinement study showing the errors in the computed solutions at $t = 2.0$ when the exact solution is the trigonometric function (58), *with direct and smooth start.*

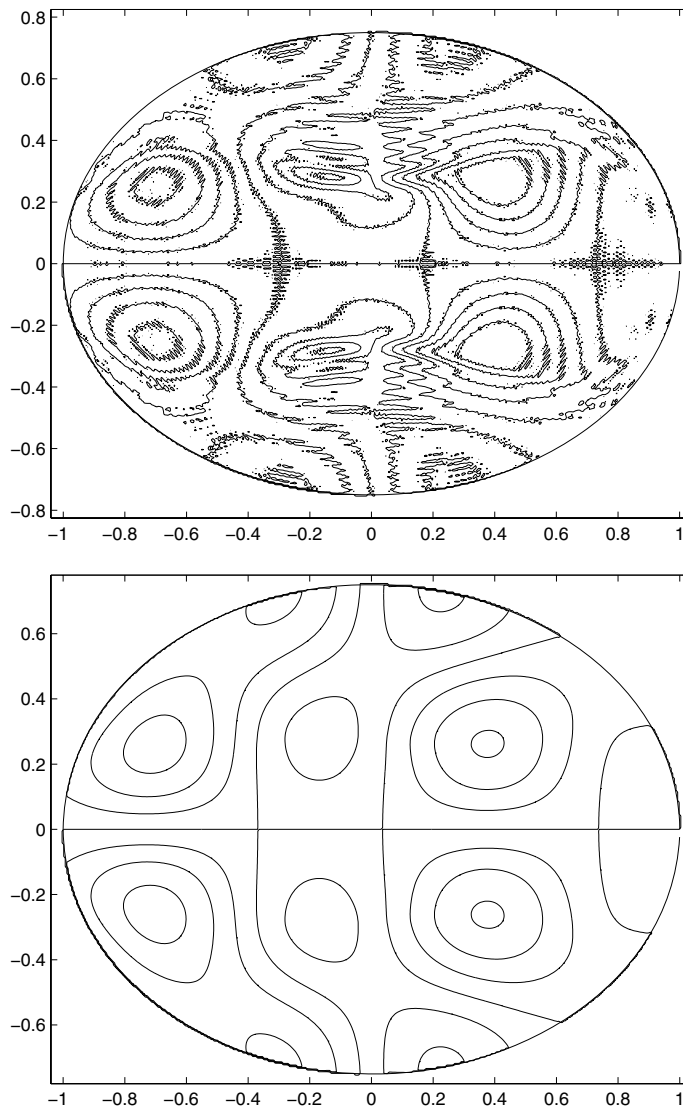|	Direct start			Smooth start		
N	$\|u_{\text{err}}\|_\infty$	$\|\nabla u_{\text{err}}\|_\infty$	$\|\Delta u_{\text{err}}\|_\infty$	$\|u_{\text{err}}\|_\infty$	$\|\nabla u_{\text{err}}\|_\infty$	$\|\Delta u_{\text{err}}\|_\infty$
201	$2.23 \cdot 10^{-3}$	$3.48 \cdot 10^{-2}$	14.3	$1.39 \cdot 10^{-3}$	$8.60 \cdot 10^{-3}$	$7.25 \cdot 10^{-2}$
401	$5.38 \cdot 10^{-4}$	$1.27 \cdot 10^{-2}$	9.86	$3.43 \cdot 10^{-4}$	$2.15 \cdot 10^{-3}$	$1.83 \cdot 10^{-2}$

FIG. 2. *Error in the solution at time $t = 2.0$, with direct start (top) and smooth start (bottom). In both cases, the grid size was $h = 2.08/400$ $(N = 401)$ and $CFL = 0.5$. Contours are equally spaced in $[-4 \cdot 10^{-4}, 4 \cdot 10^{-4}]$ with step size 10^{-4}.*
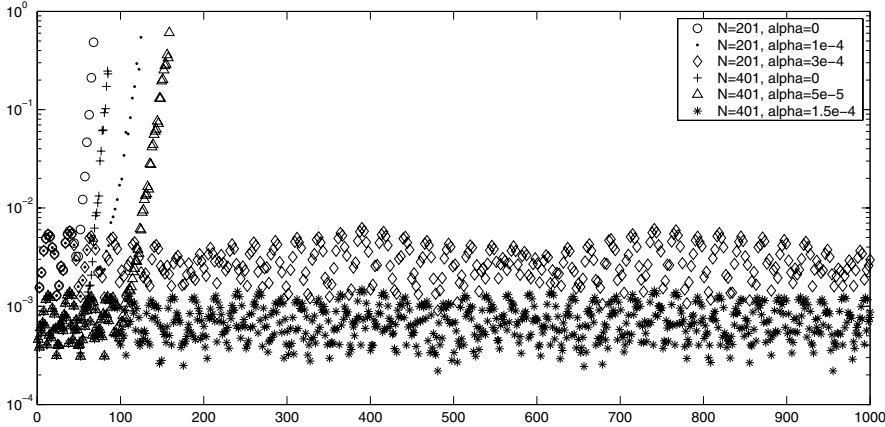
FIG. 3. *Max error in the solution as a function of time for different damping coefficients α and grid sizes N. For $N = 401$, time 1000 was reached after taking $384,615$ time steps.*

Next we investigate the long-time properties of the time-integration scheme. In Figure 3 we report the error in the solution for different values of the damping coefficient α and for grid sizes $N = 201$ and $N = 401$. The domain is the same ellipse as before, CFL $= 0.5$, and smooth start is enabled. Damping is clearly needed to reach time 1000, corresponding to $384,615$ time steps on the finer grid, and we need to take $\alpha = 3 \cdot 10^{-4}$ to stabilize the scheme for the coarse grid. However, for the finer grid it suffices with $\alpha = 1.5 \cdot 10^{-4}$. This suggests that $\alpha = h\tilde{\alpha}$; i.e., the damping term can be of the order $\mathcal{O}(h^4)$. Note that there is no apparent increase in the error after long times, which indicates that the damping is very mild and that the scheme is appropriate for long time computations.

4.2. The TM_z problem. We proceed by testing our method on the TM_z problem for Maxwell's equations, i.e., the two-dimensional case where

$$\boldsymbol{H} = H^{(x)}(x, y, t)\boldsymbol{e}_x + H^{(y)}(x, y, t)\boldsymbol{e}_y$$

and $\boldsymbol{E} = E^{(z)}(x, y, t)\boldsymbol{e}_z$. By scaling the dependent variables and time, Maxwell's equations describing a homogeneous, lossless material without charges simplify to (cf. [15])

$$(59) \qquad \frac{\partial H^{(x)}}{\partial t} = -\frac{\partial E^{(z)}}{\partial y},$$

$$(60) \qquad \frac{\partial H^{(y)}}{\partial t} = \frac{\partial E^{(z)}}{\partial x} \qquad \text{in } \Omega, \quad t \geq 0,$$

$$(61) \qquad \frac{\partial E^{(z)}}{\partial t} = \frac{\partial H^{(y)}}{\partial x} - \frac{\partial H^{(x)}}{\partial y},$$

subject to the constraint

$$(62) \qquad \frac{\partial H^{(x)}}{\partial x} + \frac{\partial H^{(y)}}{\partial y} = 0 \quad \text{in } \Omega, \quad t \geq 0.$$

By cross-differentiation,

$$
\text{(63)} \qquad \frac{\partial^2 E^{(z)}}{\partial t^2} = \frac{\partial^2 E^{(z)}}{\partial x^2} + \frac{\partial^2 E^{(z)}}{\partial y^2} \quad \text{in } \Omega, \quad t \geq 0.
$$

The perfectly electric conducting (PEC) boundary condition $\boldsymbol{n} \times \boldsymbol{E} = 0$, where $\boldsymbol{n} = n^{(x)}\boldsymbol{e}_x + n^{(y)}\boldsymbol{e}_y$ is the outward normal of the boundary, becomes

$$
(\boldsymbol{e}_x n^{(y)} - \boldsymbol{e}_y n^{(x)})E^{(z)} = 0 \quad \text{on } \Gamma,
$$

i.e.,

$$
\text{(64)} \qquad E^{(z)} = 0 \quad \text{on } \Gamma.
$$

Instead of directly solving the first order system (59)–(61), we solve the second order equation (63) subject to the Dirichlet boundary condition (64). Once $E^{(z)}$ is computed, the equations for $H^{(x)}$ and $H^{(y)}$, (59) and (60), reduce to ordinary differential equations at each point in Ω.

On the discrete side, (59) and (60) are integrated in time using the second order Adams–Bashforth method:

$$
\text{(65)} \qquad H_{i,j}^{(x)}(t_{n+1}) = H_{i,j}^{(x)}(t_n) - \frac{k}{2}\left(3D_0^y E_{i,j}^{(z)}(t_n) - D_0^y E_{i,j}^{(z)}(t_{n-1})\right),
$$

$$
\text{(66)} \qquad H_{i,j}^{(y)}(t_{n+1}) = H_{i,j}^{(y)}(t_n) + \frac{k}{2}\left(3D_0^x E_{i,j}^{(z)}(t_n) - D_0^x E_{i,j}^{(z)}(t_{n-1})\right).
$$

As a result, the following second order accurate centered approximation of the divergence constraint (62) satisfies

$$
D_0^x H_{i,j}^{(x)}(t_n) + D_0^y H_{i,j}^{(y)}(t_n) = D_0^x H_{i,j}^{(x)}(0) + D_0^y H_{i,j}^{(y)}(0), \quad t_n > 0.
$$

Hence, if the discrete divergence is initially zero, it will remain so for all subsequent times.

We use the scheme (19) together with the smooth start procedure to evolve (63). This is a good test of the numerical accuracy of $E^{(z)}$, since $H^{(x)}$ and $H^{(y)}$ depend on the gradient of $E^{(z)}$. Initial conditions for (59)–(61) are $H^{(x)}(\boldsymbol{x}, 0)$, $H^{(y)}(\boldsymbol{x}, 0)$, and $E^{(z)}(\boldsymbol{x}, 0)$. The second order formulation (63) also needs the time derivative of $E^{(z)}$ at $t = 0$. This follows from (61):

$$
E_t^{(z)}(\boldsymbol{x}, 0) = H_x^{(y)}(\boldsymbol{x}, 0) - H_y^{(x)}(\boldsymbol{x}, 0).
$$

Furthermore, to start the Adams–Bashforth scheme (65)–(66), we need an accurate approximation of $E^{(z)}(\boldsymbol{x}_{i,j}, -k)$:

$$
E^{(z)}(\boldsymbol{x}_{i,j}, -k) = E^{(z)}(\boldsymbol{x}_{i,j}, 0) - kE_t^{(z)}(\boldsymbol{x}_{i,j}, 0) + \frac{k^2}{2}\Delta_h E^{(z)}(\boldsymbol{x}_{i,j}, 0).
$$

When Ω is a unit circular disc, Maxwell's equations can be solved analytically using separation of variables using polar coordinates (ρ, θ):

$$
x(\rho, \theta) = \rho \cos \theta,
$$
$$
y(\rho, \theta) = \rho \sin \theta.
$$

TABLE 4
Error in the computed solution of the TM_z problem for the mode $m = 3$, $n = 1$ at time $t = 2.0$.

	Direct start					
N	$\|E^{(z)}_{\text{error}}\|_\infty$	$\|H^{(x)}_{\text{error}}\|_\infty$	$\|H^{(y)}_{\text{error}}\|_\infty$	$\|E^{(z)}_{x\,\text{error}}\|_\infty$	$\|E^{(z)}_{y\,\text{error}}\|_\infty$	$\|\Delta E^{(z)}_{\text{error}}\|_\infty$
201	$1.03 \cdot 10^{-3}$	$1.47 \cdot 10^{-3}$	$1.98 \cdot 10^{-3}$	$1.32 \cdot 10^{-2}$	$1.63 \cdot 10^{-2}$	$8.52 \cdot 10^{0}$
401	$2.53 \cdot 10^{-4}$	$3.54 \cdot 10^{-4}$	$4.90 \cdot 10^{-4}$	$3.99 \cdot 10^{-3}$	$4.77 \cdot 10^{-3}$	$4.02 \cdot 10^{0}$
	Smooth start					
201	$1.59 \cdot 10^{-3}$	$3.93 \cdot 10^{-3}$	$3.28 \cdot 10^{-3}$	$2.61 \cdot 10^{-3}$	$5.53 \cdot 10^{-3}$	$4.22 \cdot 10^{-2}$
401	$3.95 \cdot 10^{-4}$	$1.08 \cdot 10^{-3}$	$8.41 \cdot 10^{-4}$	$6.58 \cdot 10^{-4}$	$1.54 \cdot 10^{-3}$	$1.06 \cdot 10^{-2}$

We can alternatively express $\boldsymbol{H}$ in terms of its Cartesian or polar components, related by

$$H^{(x)} = H^{(\rho)} \cos\theta - H^{(\theta)} \sin\theta,$$
$$H^{(y)} = H^{(\rho)} \sin\theta + H^{(\theta)} \cos\theta.$$

Let $J_m(\xi)$ denote the Bessel function of the first kind of order m $(m = 0, 1, 2, \dots)$ and let $\mathcal{X}_{mn}$ be the nth zero of J_m $(n = 1, 2, 3, \dots)$, i.e., $J_m(\mathcal{X}_{mn}) = 0$, $0 < \mathcal{X}_{m1} < \mathcal{X}_{m2} < \cdots$. In terms of polar coordinates and components, the TM_z problem is solved by (cf. [15])

$$(67) \qquad E^{(z)}_{mn}(\rho, \theta) = \mathcal{X}_{mn} J_m(\mathcal{X}_{mn}\rho) \cos(m\theta) \cos(\mathcal{X}_{mn}t),$$

$$(68) \qquad H^{(\rho)}_{mn}(\rho, \theta) = \frac{m}{\rho} J_m(\mathcal{X}_{mn}\rho) \sin(m\theta) \sin(\mathcal{X}_{mn}t),$$

$$(69) \qquad H^{(\theta)}_{mn}(\rho, \theta) = \mathcal{X}_{mn} J'_m(\mathcal{X}_{mn}\rho) \cos(m\theta) \sin(\mathcal{X}_{mn}t).$$

Since the equations are linear, any linear combination of the above solution is also a solution.

We evaluate the numerical scheme by solving the TM_z problem on a unit circular disc and compare the numerical solution to the exact analytic solution (67)–(69). We consider the case $m = 3$, $n = 1$, where $\mathcal{X}_{31} \approx 6.3801618959$. The problem is discretized on a computational grid with grid size $h = 2.08/(N-1)$ and CFL $= 0.5$. In this computation, the coefficient of the artificial term in the Dirichlet boundary condition is $\gamma = 0.2$. No stabilization is necessary for these short time computations, and we set $\alpha = 0$. In Table 4 we compare the errors when the computation is started directly (from inhomogeneous initial data) and smoothly. In both cases, the errors in $E^{(z)}$, $H^{(x)}$, $H^{(y)}$, $E^{(z)}_x$, and $E^{(z)}_y$ are all $\mathcal{O}(h^2)$. However, the errors in $\Delta E^{(z)}$ reveal a highly oscillatory component in $E^{(z)}$ when the computation is started directly. Since $\partial\boldsymbol{H}/\partial t$ depends on the gradient of $E^{(z)}$, it is surprising that the errors in $\boldsymbol{H}$ are smaller when the computation is started directly, since the errors in the gradient of $E^{(z)}$ are smaller when the smooth start procedure is used.

In terms of our scaled variables, the total field energy within Ω is

$$(70) \qquad E_{\text{field}}(t) = \int_\Omega \boldsymbol{E} \cdot \boldsymbol{E} + \boldsymbol{H} \cdot \boldsymbol{H} \, d\Omega.$$

Maxwell's equations (59)–(61) subject to a homogeneous PEC boundary condition (64) imply $E_{\text{field}}(t) = E_{\text{field}}(0)$, $t > 0$. Since our scheme uses damping to ensure
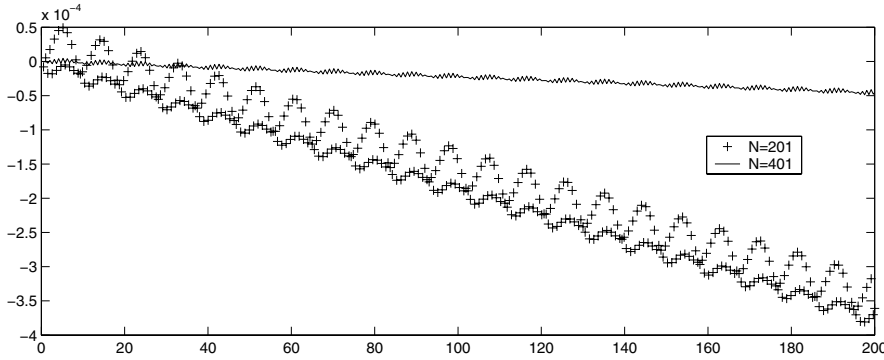
FIG. 4. *The error in the relative energy $E_{\text{field}}(t)/E_{\text{field}}(0)$ as a function of time for a circular domain for the mode $m = 3$, $n = 1$ of (67)–(69).*

stability, it is of interest to evaluate how well the energy (70) is conserved by the numerical approximation.

To evaluate (70), we need to integrate a grid function defined on the embedded boundary grid. Let $g(\boldsymbol{x})$ be a smooth function defined in Ω and take

$$g_{i,j} = \begin{cases} g(\boldsymbol{x}_{i,j}), & \boldsymbol{x}_{i,j} \in \Omega, \\ \text{extrap}(g)_{i,j}, & \boldsymbol{x}_{i,j} \notin \Omega, \ \boldsymbol{x}_{i\pm1,j} \in \Omega \text{ or } \boldsymbol{x}_{i,j\pm1} \in \Omega, \\ 0, & \text{otherwise,} \end{cases}$$

where $\text{extrap}(g)_{i,j}$ is defined by linear extrapolation from the interior points. We approximate the integral by a sum of grid cell averages of g:

$$(71) \qquad \int_\Omega g(\boldsymbol{x}) \, d\Omega \approx \sum_{i,j} C_{i+1/2,j+1/2} \frac{g_{i,j} + g_{i+1,j} + g_{i,j+1} + g_{i+1,j+1}}{4}.$$

For interior cells where all four grid vertices are inside Ω, the cell area is $C_{i+1/2,j+1/2} = h^2$. When all four grid vertices are outside Ω, the cell area is $C_{i+1/2,j+1/2} = 0$. For cells cut by the boundary, we first compute the intersections between the boundary and the four grid lines x_i, x_{i+1}, y_j, y_{j+1}. To estimate the cell area, the cell boundary is approximated by a linear segment between each intersection point. This procedure together with the linear extrapolation to define $\text{extrap}(g)$ in points just outside the boundary has been verified to give a second order accurate quadrature formula.

In Figure 4 we plot the error in the relative energy $E_{\text{field}}(t)/E_{\text{field}}(0)$ as a function of time for a circular domain. As before, we study the mode $m = 3$, $n = 1$ and use the same parameters as before. For these long time computations, the stabilization term is necessary and we set $\alpha = 10^{-3}$. As can be expected, the conservation error is $\mathcal{O}(h^2)$ and grows approximately linearly in time. For the fine mesh, the relative energy is conserved to within $5 \cdot 10^{-5}$ at time $t = 200$, and we conclude that the effect of the stabilization term is very small.

Next we study the evolution of a pulse centered at $(x, y) = (x_F, y_F)$ in a more complicated region where the boundary is represented by a cubic spline; see Figure 5. We start the computation from a localized perturbation in $E^{(z)}$ near (x_F, y_F):

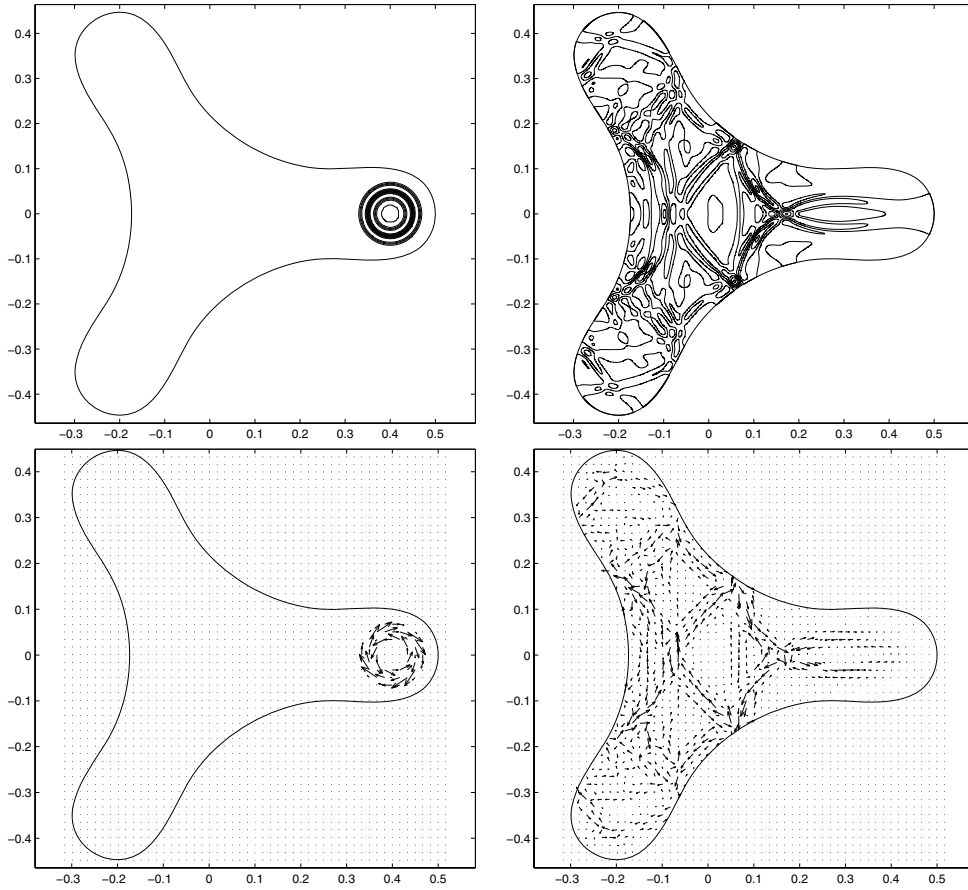$$E^{(z)}(x, y, 0) = \phi(\sqrt{(x - x_F)^2 + (y - y_F)^2}).$$

FIG. 5. *The evolution of $E^{(z)}$ (top) and $\boldsymbol{H}$ (bottom) in the problem for the grid refinement test. The left-hand figures show initial data and the right-hand figures show the solution at time $t = 0.8$. The solutions are shown on the finest grid with 1601×1790 grid points. Contours are spaced equally in $[-1.0, 1.0]$ with step size 0.2. Every 32nd grid point is used in the vector plots in the bottom row.*

To make the perturbation propagate (essentially) radially outward from (x_F, y_F), we take

$$\frac{\partial E^{(z)}}{\partial t}(x, y, 0) = -\phi'(\sqrt{(x - x_F)^2 + (y - y_F)^2}).$$

However, to start the computation we must specify compatible initial data for $\boldsymbol{H}$. Let $\psi(x, y)$ be a scalar field. The initial $\boldsymbol{H}$ field will be divergence free if

$$(72) \qquad\qquad\qquad H^{(x)}(x, y, 0) = -\frac{\partial \psi}{\partial y},$$

$$(73) \qquad\qquad\qquad H^{(y)}(x, y, 0) = \frac{\partial \psi}{\partial x}.$$

Note that (61) yields

$$\frac{\partial E^{(z)}}{\partial t}(x, y, 0) = \Delta \psi.$$

Hence, we can find the initial data for $(E^{(x)}, E^{(y)})$ by solving the Poisson problem

$$(74) \qquad \Delta \psi = -\phi'$$

and inserting the gradient of ψ in (72)–(73). In special cases, this can be done analytically. Introduce polar coordinates (ρ, θ) centered around the point (x_F, y_F),

$$x = x_F + \rho \cos \theta,$$
$$y = y_F + \rho \sin \theta,$$

and let ϕ be independent of θ, i.e., $\phi = \phi(\rho)$. The solution of (74) is then

$$(75) \qquad \psi_\rho(\rho) = -\phi(\rho) + \frac{1}{\rho} \int_0^\rho \phi(\rho')\, d\rho',$$

and since ψ is independent of θ, $\psi_x = (x - x_F)\psi_\rho/\rho$ and $\psi_y = (y - y_F)\psi_\rho/\rho$. If we take

$$\phi(\rho) = \begin{cases} 0, & \rho < r_0, \\ P\left(\frac{\rho - r_0}{r_1 - r_0}\right), & r_0 \leq \rho \leq r_1, \\ 0, & r > r_1, \end{cases} \qquad P(\xi) = a\xi^5(1 - \xi)^5(\xi - 1/2),$$

we have $\int_0^1 P(\xi)\, d\xi = 0$, and thus $\psi_\rho(\rho)$ has compact support in $r_0 \leq \rho \leq r_1$.

In the computation shown in Figure 5, we used $x_F = 0.4$, $y_F = 0$, $r_0 = 0.02$, and $r_1 = 0.08$ to give the initial data compact support inside Ω, and set $a = 10938.8$, which normalizes the initial data to $-1 \leq E^{(z)}(x, y, 0) \leq 1$. Since the initial data have compact support, the smooth start procedure was not necessary in this computation. No exact solution is known for this problem and we resort to a grid refinement study to access the accuracy of the computed solution. Three calculations were performed where the grid size was $h = 5.193 \cdot 10^{-4}$, $2h$, and $4h$, respectively. The corresponding grids had 1601×1790, 801×896, and 401×448 grid points, respectively. In this computation, we used $\alpha = 10^{-3}$, $\gamma = 0.25$, and CFL $= 0.5$. Let $(E_h^{(z)}, H_h^{(x)}, H_h^{(y)})$ be the discrete solutions corresponding to grid size h. If the discrete solution is resolved on the grid, we expect it to satisfy

$$E_h^{(z)}(x_i, y_j, t_n) = E^{(z)}(x_i, y_j, t_n) + h^2 R(x_i, y_j, t_n) + \mathcal{O}(h^3)$$

and similar expressions for $H_h^{(x)}$ and $H_h^{(y)}$. Hence,

$$\frac{\|E_h^{(z)} - E_{4h}^{(z)}\|_\infty}{\|E_h^{(z)} - E_{2h}^{(z)}\|_\infty} \to 5, \quad h \to 0,$$

and corresponding expressions for $H_h^{(x)}$ and $H_h^{(y)}$. In Table 5, we report the calculated convergence rates at time $t = 0.8$. The calculated rates are near the asymptotic value of 5, which indicates that the solution is second order accurate. The relatively large difference between the solution on the fine and coarse grids indicates that the solution on that grid is not very accurate, despite being in the asymptotic range.

For completeness, we give the (x, y)-coordinates of the 21 node points in the periodic interpolating cubic spline: $(-0.0384, -0.2665)$; $(0.25, -0.1)$; $(0.4, -0.1)$; $(0.4707, -0.0707)$; $(0.5, 0.0)$; $(0.4707, 0.0707)$; $(0.4, 0.1)$; $(0.25, 0.1)$; $(-0.0384, 0.2665)$; $(-0.1134, 0.3964)$; $(-0.1741, 0.443)$; $(-0.25, 0.433)$; $(-0.2966, 0.3722)$; $(-0.2866, 0.2964)$; $(-0.2116, 0.1665)$; $(-0.2116, -0.1665)$; $(-0.2866, -0.2964)$; $(-0.2966, -0.3722)$; $(-0.25, -0.433)$; $(-0.1741, -0.443)$; and $(-0.1134, -0.3964)$.

TABLE 5
Convergence of the discrete solution.

	$X = E^{(z)}$	$X = H^{(x)}$	$X = H^{(y)}$
$\|X_h - X_{4h}\|_\infty$	0.3636	0.3552	0.2491
$\|X_h - X_{2h}\|_\infty$	0.0744	0.0621	0.0622
Ratio	4.89	5.24	4.00

5. Conclusions. We have developed a Cartesian embedded boundary method for the second order wave equation in general two-dimensional domains subject to Dirichlet boundary conditions, where both the solution and its gradient are second order accurate. By adding a small artificial term to the discrete boundary condition, we avoid the small-cell stiffness problem and can use an explicit time-integration method where the time step essentially equals that of a periodic domain.

Work is under way to solve Maxwell's equations written as a system of second order wave equations by combining the current method with our previous method for the Neumann problem [2]. Future developments include treatment of discontinuous wave propagation speeds, unbounded domains (far field boundaries), and generalizations to three space dimensions.

Appendix A. Estimating γ in the Dirichlet boundary condition.
Consider the semidiscrete one-dimensional wave equation (27)–(29). After eliminating the ghost point v_0, we can write the system in matrix form as follows:

$$\boldsymbol{v}_{tt} = A\boldsymbol{v} + \boldsymbol{F} + \boldsymbol{b}, \quad \boldsymbol{v} = (v_1, v_2, v_3, \dots)^T .$$

As before, $\boldsymbol{F}$ and $\boldsymbol{b}$ are the interior and boundary forcing terms, respectively. The tridiagonal matrix A satisfies

$$A = \frac{1}{h^2} \begin{pmatrix} -2 - \frac{c_1 - 2\gamma}{c_0 + \gamma} & 1 - \frac{c_2 + \gamma}{c_0 + \gamma} & 0 & 0 & \cdots \\ 1 & -2 & 1 & 0 & \cdots \\ 0 & 1 & -2 & 1 & \\ \vdots & & \ddots & \ddots & \ddots \end{pmatrix}.$$

Let the eigenvalues of A be λ_j. Since A can be symmetrized by a diagonal matrix, all eigenvalues of A are real valued. For all rows except the first, the Gershgorin circles (see, e.g., [16]) for the matrix $h^2 A$ are

$$\Lambda_j = \{z : |z + 2| \le 2\}, \quad j \ge 2,$$

that is, a circle in the complex z-plane with radius 2 centered at $z = -2$. The circle corresponding to the first row is

$$\Lambda_1 = \left\{ z : \left| z + 2 + \frac{c_1 - 2\gamma}{c_0 + \gamma} \right| \le 1 - \frac{c_2 + \gamma}{c_0 + \gamma} \right\}.$$

Since all eigenvalues of A are real, the circles correspond to intervals on the real axis, and the Gershgorin circle theorem says that all eigenvalues of A are located in the union of these intervals.

We begin by demonstrating the small-cell stiffness when $\gamma = 0$ and $\beta \to 0$. In this case, the Gershgorin circle from the first row in A is disjoint from the remaining circles when $0 \le \beta < (\sqrt{3} - 1)/2$. For such β, there must be one eigenvalue of A that lies within the interval

$$-3 - \frac{c_1 - c_2}{c_0} \le h^2 \lambda_1 \le -1 - \frac{c_1 + c_2}{c_0},$$

and we conclude that $h^2 \lambda_1 \to -\infty$ as $\beta \to 0$. As a result, the CFL condition for the explicit time integration scheme (37) becomes $k/h \to 0$ as $\beta \to 0$; see [1].

Next, we want to estimate the eigenvalue with the largest magnitude for $\gamma > 0$. The interval corresponding to all circles except the first is $-4 \le \Re(z) \le 0$ and the interval from Λ_1 is

$$-3 - \frac{c_1 - c_2 - 3\gamma}{c_0 + \gamma} \le \Re(z) \le -1 + \frac{\gamma - c_1 - c_2}{c_0 + \gamma}.$$

Hence, we study how large

$$q(\beta, \gamma) = \frac{c_1(\beta) - c_2(\beta) - 3\gamma}{c_0(\beta) + \gamma}$$

can be for $0 \le \beta \le 1$, $\gamma > 0$. The coefficients in q are given by (26). When $\gamma \le 0.25$, the maximum of q is attained at $\beta = 0$ and satisfies

(76)
$$\max_{0 \le \beta \le 1} q(\beta, \gamma) = q(0, \gamma) = \frac{1 - 3\gamma}{\gamma}, \quad \gamma \le 0.25.$$

For $\gamma > 0.25$, $\max q(\beta, \gamma) < q(0, 0.25)$. Hence, to obtain the same lower bound from the first Gershgorin circle as from the rest, we require $\max q \le 1$ and (76) gives $\gamma \ge 0.25$. The upper bound from Λ_1 is always less than zero for $0 \le \beta \le 1$. Hence, all eigenvalues of A satisfy the estimate

$$-4 \le h^2 \lambda_j \le 0 \quad \text{for } \gamma \ge 0.25,$$

and the CFL condition for the explicit time integration scheme (37) becomes $k/h < 1$, see [1].

REFERENCES

[1] H.-O. KREISS, N. A. PETERSSON, AND J. YSTRÖM, *Difference approximations for the second order wave equation*, SIAM J. Numer. Anal., 40 (2002), pp. 1940–1967.

[2] H.-O. KREISS, N. A. PETERSSON, AND J. YSTRÖM, *Difference approximations of the Neumann problem for the second order wave equation*, SIAM J. Numer. Anal., 42 (2004), pp. 1292–1323.

[3] B. GUSTAFSSON, H.-O. KREISS, AND J. OLIGER, *Time Dependent Problems and Difference Methods*, Wiley–Interscience, New York, 1995.

[4] G. BROWNING, H-.O. KREISS, AND J. OLIGER, *Mesh refinement*, Math. Comp., 27 (1973), pp. 29–39.

[5] R. WELLER AND G. H. SHORTLEY, *Calculation of stresses within the boundary of photoelastic models*, J. Appl. Mech., 6 (1939), pp. A-71–A-78.

[6] L. COLLATZ, *The Numerical Treatment of Differential Equations*, 3rd ed., Springer-Verlag, Berlin, 1960.

[7] R. B. PEMBER, J. B. BELL, P. COLELLA, W. Y. CRUTCHFIELD, AND M. L. WELCOME, *An adaptive Cartesian grid method for unsteady compressible flow in irregular regions*, J. Comput. Phys., 120 (1995), pp. 278–304.

[8] M. J. Berger, C. Helzel, and R. J. LeVeque, *h-Box methods for the approximation of hyperbolic conservation laws on irregular grids*, SIAM J. Numer. Anal., 41 (2003), pp. 893–918.

[9] C. Zhang and R. LeVeque, *The immersed interface method for acoustic wave equations with discontinuous coefficients*, Wave Motion, 25 (1997), pp. 237–263.

[10] A. Ditkowski, K. Dridi, and J. S. Hesthaven, *Convergent Cartesian grid methods for Maxwell's equations in complex geometries*, J. Comput. Phys., 170 (2001), pp. 39–80.

[11] H. Johansen and P. Colella, *A Cartesian grid embedded boundary method for Poisson's equation on irregular domains*, J. Comput. Phys., 147 (1998), pp. 60–85.

[12] J.-R. Li and L. Greengard, *High order marching schemes for the wave equation in complex geometry*, J. Comput. Phys., 198 (2004), pp. 295–309.

[13] H.-O. Kreiss and J. Lorenz, *Initial-Boundary Value Problems and the Navier-Stokes Equations*, Academic Press, San Diego, 1989.

[14] D. Gilbarg and N. S. Trudinger, *Elliptic Partial Differential Equations of Second Order*, Springer-Verlag, Berlin, 1983.

[15] C. A. Balanis, *Advanced Engineering Electromagnetics*, Wiley, New York, 1989.

[16] G. H. Golub and J. M. Ortega, *Scientific Computing and Differential Equations*, Academic Press, San Diego, 1992.